Chemical Geology 618 (2023) 121300

Contents lists available at ScienceDirect

Chemical Geology

journal homepage: www.elsevier.com/locate/chemgeo

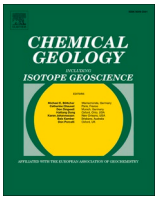

Trace metals as a redox proxy in Arabian Sea sediments in and below the oxygen minimum zone

Annika Vollebregt [a], Niels A.G.M. van Helmond [a,b,*], Susan Pit [a,c], Peter Kraal [a,d], Caroline P. Slomp [a,b]

[a] Department of Earth Sciences - Geochemistry, Faculty of Geosciences, Utrecht University, Princetonlaan 8a, 3584 CB Utrecht, the Netherlands
[b] Radboud Institute of Biological and Environmental Sciences, Radboud University, Nijmegen, the Netherlands
[c] Department of Earth and Planetary Sciences, University of California at Santa Cruz, USA
[d] Department of Ocean Systems, Royal Netherlands Institute for Sea Research, P.O. Box 59, 1790 AB Den Burg, the Netherlands

ARTICLE INFO

Editor: Karen Johannesson

Keywords:
Molybdenum
Uranium
Iron
Manganese
Redox transect
Murray Ridge

ABSTRACT

Sedimentary trace metals are widely used to reconstruct past bottom water redox conditions. The calibration of trace metals as a redox proxy for oxygen minimum zones (OMZs) can still be improved. Here, we combine pore water and solid phase Mo, U, Re and V profiles with Fe and Mn data for ten sites along a bottom water oxygen (2 to 83 μmol L^{-1} O_2) and water depth gradient (885 to 3010 m) in and below the perennial OMZ in the northern Arabian Sea (Murray Ridge). Trends in sedimentary Mo, U and Re contents generally follow ambient bottom water redox conditions, with the highest enrichments in OMZ sediments, supporting the validity of these trace metals as redox proxies. Vanadium and Fe are exclusively enriched in the sediments of the most anoxic OMZ site and do not capture further redox changes in and below the OMZ. We attribute the absence of a redox trend in sedimentary Fe content to the mildly reducing conditions in the sediments, with little FeS formation and benthic release of Fe. Manganese, in contrast, is depleted in the OMZ sediments and enriched in sediments below the OMZ, in accordance with loss from OMZ sediments and transfer of Mn to deeper sites ("Mn shuttling"). Manganese oxides are likely a key carrier of Mo and V to the sediments, especially below the OMZ, while diffusion across the sediment-water interface supplies U. Sedimentary Mo, U and V contents in the present-day Arabian Sea OMZ are generally lower than observed in other perennial OMZs. This may be related to a lower input of organic matter in this part of the Arabian Sea when compared to other OMZs, and hence, less anaerobic degradation of organic matter and less authigenic fixation of metals, even at the same bottom water oxygen concentrations. Our results have implications for the detection of OMZs in the geological record, implying that thresholds in trace metal concentrations for perennial OMZs may be lower than previously considered. Comparison of our Mo, U, Re and V data to trace metal records from 15 to 200 ka for the same Arabian Sea region suggests that the OMZ was periodically wider and more reducing in the past.

1. Introduction

Various trace metals such as Mo, U, Re and V are enriched in sediments under low-oxygen conditions (e.g. Lyons and Severmann, 2006; Morford and Emerson, 1999), making them highly suitable as paleo-redox proxies (McManus et al., 2006; Raiswell et al., 2018; Scholz, 2018; Algeo and Li, 2020). As a consequence, trace metal records are frequently used in reconstructions of past redox conditions in the ocean (e.g. Brumsack, 1989; van der Weijden et al., 2006; Tribovillard et al., 2006; van Helmond et al., 2018). Such reconstructions, when applied to past oceans in a warmer climate, provide important context for the present-day expansion of oceanic oxygen minimum zones (OMZs; Stramma et al., 2008; Schmidtko et al., 2017; Breitburg et al., 2018).

The application of trace metal proxies requires careful calibration in modern day low oxygen settings. Such calibration studies for OMZs and stratified anoxic basins have revealed distinct temporal and spatial trends in the sedimentary enrichment of trace metals as a function of bottom water redox conditions (e.g. Crusius et al., 1996; Morford and

* Corresponding author at: Department of Earth Sciences - Geochemistry, Faculty of Geosciences, Utrecht University, Princetonlaan 8a, 3584 CB Utrecht, the Netherlands.
E-mail addresses: n.vanhelmond@uu.nl (N.A.G.M. van Helmond), supit@ucsc.edu (S. Pit), peter.kraal@nioz.nl (P. Kraal), c.p.slomp@uu.nl (C.P. Slomp).

https://doi.org/10.1016/j.chemgeo.2022.121300
Received 22 July 2022; Received in revised form 1 November 2022; Accepted 28 December 2022
Available online 4 January 2023

Emerson, 1999; Bennett and Canfield, 2020; Algeo and Li, 2020). Importantly, trends in trace metal contents typically also reflect variations in environmental conditions other than bottom water redox. Examples include variations in the supply of Mn and Fe oxides and/or organic matter, which all can modulate the input and/or authigenic fixation of trace metals (Nameroff et al., 2002; Zheng et al., 2002; Algeo and Tribovillard, 2009; Helz, 2022).

Such modulation likely affects the sequestration of most trace metals, but is particularly well-described for Mo and U. When dissolved sulfide concentrations are in excess of 11 μmol L^{-1}, molybdate, (MoO_4^{2-}) is sequentially transformed into particle reactive Mo-sulfide species such as thiomolybdate, Mo polysulfide and/or iron-Mo-sulfides. When sulfide is absent, or below 11 μmol L^{-1}, molybdate diffuses into the sediments and is then scavenged via iron-Mo-sulfides, and possibly, organic matter (Helz et al., 1996; Zheng et al., 2000; Helz and Vorlicek, 2019). In settings where Mn or Fe oxides act as a carrier of Mo to the sediment, burial fluxes of Mo can be enhanced, potentially even leading to a misclassification of sediments deposited under an anoxic water column as being from a euxinic setting (Algeo and Lyons, 2006; Algeo and Tribovillard, 2009; Sulu-Gambari et al., 2017). Uranium, which is predominantly present as calcium/magnesium-uranyl-carbonate complexes in oxic seawater (e.g. Endrizzi and Rao, 2014), typically precipitates as uraninite (UO_2) in the Fe oxide reduction zone. The removal induces a gradient in dissolved U between the sediment-water interface and the Fe oxide reduction zone which allows for continued delivery of dissolved U through diffusion from the water column (Cochran et al., 1986; McManus et al., 2005; Morford et al., 2009). Variations in input of organic matter and Fe oxides can modulate the sediment enrichment of U by altering the position of the depth of the zone of sequestration and, hence, the rate of diffusive U supply (McManus et al., 2005; Morford et al., 2005). This implies that there is not necessarily a direct link between bottom water oxygen and sediment U enrichment. There is also a potential flux of Mo and U into the sediments associated with organic matter when the water column is anoxic (e.g. Zheng et al., 2002; Scholz, 2018) that remains poorly quantified.

The early diagenesis of Re and V is less well-understood but both elements are known to be enriched in sediments under anoxic bottom waters (Calvert and Pedersen, 1993). Rhenium diffuses into the sediment from overlying waters (Crusius et al., 1996; Morford et al., 2005) and/or is supplied in particulate form and released to the pore water (e.g. Helz, 2022). Rhenium is fixed authigenically in the absence of sulfide. Sedimentary enrichments of Re typically show a positive correlation with rates of organic carbon respiration (Morford et al., 2012). For V, the main supply to the sediment is thought to occur as adsorbed V on settling Mn and Fe oxides (Wehrli and Stumm, 1989), but organic matter might also act as a source (Ho et al., 2018; Scholz, 2018). Vanadium can be trapped in the sediment upon release from these solid phase carriers, with the retention being most effective in the presence of sulfide (Morford and Emerson, 1999).

The above implies that there is not necessarily a direct quantitative link between sediment trace metal contents and bottom water redox that is valid across depositional systems (Algeo and Li, 2020). Nevertheless, various quantitative thresholds have been proposed for the interpretation of trace metal records in the context of bottom water redox conditions (e.g. Scott and Lyons, 2012; Moffitt et al., 2015). In a recent study, Bennett and Canfield (2020) identified distinct groups and corresponding thresholds for a range of sediments including perennial OMZs which were characterized by Mo/Al, U/Al and V/Al ratios >46, 5 and 5 ppm/wt%, respectively. This classification was based on a data compilation for oxic environments, stratified euxinic basins and the OMZs in the Eastern Tropical North and South Pacific (e.g. Chilean and Peruvian margin) and Eastern Tropical South Atlantic (Namibian margin). Paleo-redox interpretations based on such thresholds can be complemented with data on sediment Mn/Al (Calvert and Pedersen, 1993; Lenz et al., 2015), Fe/Al and Fe speciation (Poulton and Canfield, 2005; Raiswell et al., 2018), both as redox proxies and to obtain insight into the role of Mn and Fe as carriers of trace metals. Further improvements can also be expected when assessing proxy data for additional marine regions.

The modern Arabian Sea OMZ, one of the major OMZs in the present ocean (Paulmier and Ruiz-Pino, 2009), is not included in current trace metal paleo-proxy calibrations, nor have the processes leading to trace metal sequestration been evaluated based on modern sediment and pore water data. Hence, long core records of Mo, U, Re and V for Arabian Sea OMZ sediments deposited from 15 to 200 ka remain uncalibrated (van der Weijden et al., 2006). A recent study of surface sediments across redox transects along the western Indian Margin (Kessarkar et al., 2022) reported Mo/Al, U/Al and V/Al values for the Arabian Sea OMZ that are consistently below the thresholds for perennial OMZ sediments as proposed by Bennett and Canfield (2020). This was attributed to as yet unknown regional factors (Kessarkar et al., 2022), illustrating the need for studies on trace metal cycling in the Arabian Sea.

Here, we present pore water and sedimentary Mn, Fe, Mo, U, Re, V data (for the solid phase, also normalized to Al) for ten sites along a bottom water oxygen and water depth transect on the Murray Ridge in the Arabian Sea. We combine the (trace) metal data with sediment Fe speciation. The goals of our research are to obtain insight into (1) potential sources of the trace metals sequestered in the sediments, including the role of Mn and Fe oxides as carriers; (2) typical ranges of trace metal contents in and below the modern Arabian Sea OMZ; and (3) the validity and applicability of the trace metals as a paleo-redox proxy in this setting, also within the context of data for other OMZs and for the Arabian Sea in the past. Our results highlight that especially Mo, U and Re are useful redox proxies in the Arabian Sea but also point towards a lower range of Mo, U and V concentrations in the OMZ sediments than observed for other perennial OMZs.

2. Materials and methods

2.1. Study area and sample sites

The Arabian Sea is located in the northern Indian Ocean and is characterized by a perennial OMZ between ±200 and ±1200 m water depth (Fig. 1). Strong south westerly monsoonal winds cause upwelling of nutrient-rich waters during the Northern-Hemisphere summer, resulting in a high surface water productivity (Qasim, 1982; Acharya and Panigrahi, 2016). The associated high downward flux of organic matter, combined with weak ventilation are responsible for the development of the OMZ, which is characterized by oxygen concentrations below 2 μmol L^{-1} in its core (Olson et al., 1993; Naqvi et al., 2010). While the upper boundary of the OMZ varies seasonally, the lower boundary is generally stable over the year (Cowie and Levin, 2009; Koho et al., 2015). The intensity and vertical extent of the OMZ varies on millennial times scales (Reichart et al., 1998).

The Murray Ridge, a bathymetric high rising ~2000 m above the seafloor on the India-Arabia plate boundary, represents an open ocean setting with a low rate of sedimentation (~2–13 cm kyr^{-1}; Koho et al., 2013). Sediment samples from Murray Ridge were obtained using a multi-corer at 10 sites along a water depth transect during an expedition in January 2009 with R/V *Pelagia* (Fig. 1; Table 1). Bottom water temperatures along the transect decreased from 10 °C at 885 m depth to 1.4 °C at 3010 m. Sites 1B and 2 are located within the nearly anoxic core of the OMZ (~2 μmol L^{-1} O_2), while the other sites are located in waters with increasing bottom water oxygen concentrations along the water depth transect, which we define here as below the OMZ (Kraal et al., 2012). Organic carbon (C_{org}) contents decrease with increasing water depth and bottom water oxygen, in accordance with the breakdown of organic matter during sinking and decreased preservation due to exposure to oxygen (Koho et al., 2013; Nierop et al., 2017). The organic matter in Murray Ridge sediments is predominantly of marine origin (e.g. Sinninghe Damsté et al., 2002; Lengger et al., 2014; Nierop et al., 2017). Biomarker studies have shown that the organic matter consists of a mixture of phytoplankton (e.g. haptophytes, diatoms,

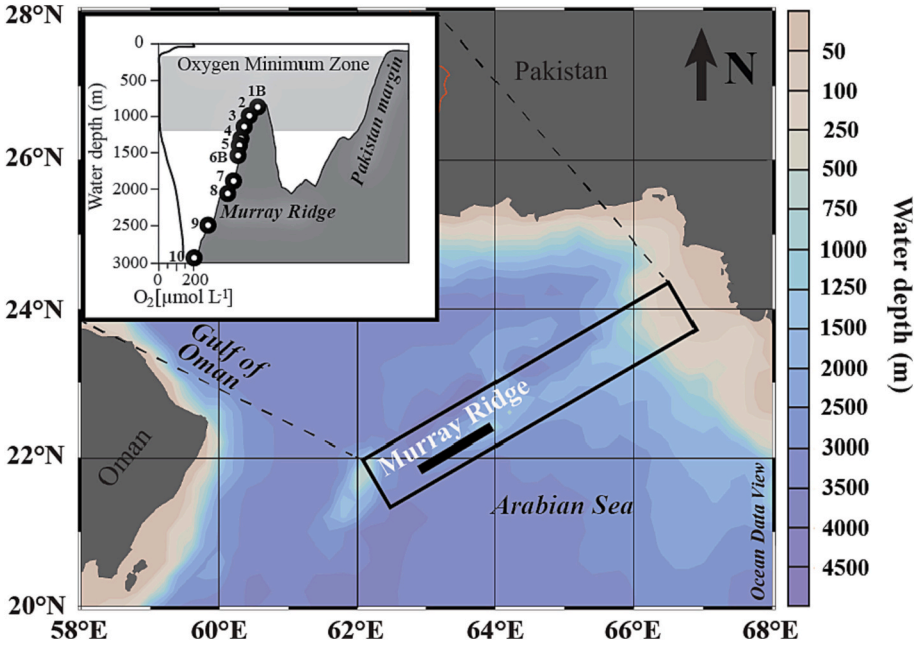

Fig. 1. Bathymetric map of the Arabian Sea with the location of the Murray Ridge indicated with a rectangle. The bold black line in the rectangle specifies the depth transect along which sampling was conducted. The inset shows a schematic representation of Murray Ridge, with the water column dissolved O_2 profile on the left and study sites indicated with circles and site numbers. This figure was made with Ocean Data View (Schlitzer, 2015).

Table 1
Site characteristics. Temperature and bottom water oxygen concentrations derived from CTD measurements as described previously (Kraal et al., 2012). Depth unit mbss is meters below sea surface. Total organic carbon (C_{org}) refers to the average for the top 2 cm ($n = 4$), with standard deviation between parentheses (data from Kraal et al., 2012).

Site	Latitude (N)	Longitude (E)	Water depth (mbss)	Temperature (°C)	Bottom water O_2 (µmol L^{-1})	C_{org} (wt %)
1B	22°32.9'	64°02.4'	885	10.0	2.0	5.6 (±0.19)
2	22°33.9'	64°03.8'	1013	8.6	2.8	4.2 (±0.04)
3	22°19.9'	63°36.0'	1172	7.8	5.0	3.6 (±0.10)
4	22°18.0'	63°36.0'	1306	6.7	14.3	2.9 (±0.08)
5	22°09.3'	63°12.8'	1379	6.5	16.5	1.4 (±0.11)
6B	22°04.7'	63°04.5'	1495	5.6	25.2	1.5 (±0.08)
7	22°18.5'	63°24.5'	1791	4.1	43.9	1.1 (±0.24)
8	22°08.7'	63°01.1'	1970	3.1	55.5	1.0 (±0.18)
9	22°06.3'	62°53.7'	2470	2.1	63.8	0.8 (±0.13)
10	22°55.6'	63°10.6'	3010	1.4	82.9	0.7 (±0.12)

dinoflagellates), bacteria and archaea (Sinninghe Damsté et al., 2002; Lengger et al., 2014). The latter is corroborated by microscopy, flow cytometry, pigment analysis and analysis of satellite data (e.g. Tarran et al., 1999; Vidya and Kurian, 2018).

2.2. Sampling

The sediment cores were visually inspected to verify that the sediment-water interface was intact. One core was sampled for sediments and pore water in a nitrogen-purged glovebox. After collection of a bottom water sample, the remaining overlying water was siphoned off and the core was sliced at a resolution of 0.5 cm, (0–2 cm), 1 cm (2–10 cm) and 2 cm until the bottom of the core. A subsample from each sediment slice was stored under nitrogen in glass 15 ml vials in an airtight larger glass vial at −20 °C. These samples were used to determine porosity and for solid phase analyses. The remaining sediment was centrifuged for 20 min at 4500 rpm to collect pore water. The supernatant was removed and filtered in the glovebox over 0.45 µm teflon filters and split into subsamples. Samples for metal analyses were acidified (10 µl concentrated ultrapure HCl per ml of sample) and stored at 4 °C. Samples for nitrate and ammonium analysis were stored at −20 °C. Samples for sulfide (0.5 ml of sample added to 1.5 ml of 8 M NaOH) and sulfate analysis were stored in glass vials at 4 °C. Samples for dissolved inorganic carbon (DIC) were stored in glass vials without headspace at 4 °C.

2.3. Analytical methods

Dissolved Mn, Fe, Mo, U, Re and V in pore water and bottom water samples were determined using an inductively coupled plasma mass spectrometer (ICP-MS, ThermoFisher Scientific Element 2-XR). The limit of detection was 18 nmol L^{-1} for Mn, 29 nmol L^{-1} for Fe, 1.3 nmol L^{-1} for Mo, 0.0012 nmol L^{-1} for U, 0.005 nmol L^{-1} for Re and 1.9 nmol L^{-1} for V. Accuracy (recovery) based on average QC yield was between 93 and 111% for all reported elements. No pore water Re data are available for sites 4 to 10. Nitrate and ammonium were measured using auto-analyzers following the imidazol method (Grasshoff et al., 1983) and phenolhypochlorite method (Helder and de Vries, 1979), respectively. Sulfate was determined using ion chromatography. Sulfide was measured spectrophotometrically following Grasshoff et al. (2009). The detection limit for H_2S was ~1 µmol L^{-1}. Replicate analyses indicated that the relative error for the pore water analyses was generally <10%.

The sediment samples were freeze-dried and ground with an agate mortar and pestle in an argon-purged glovebox. In order to determine the total elemental composition, 125 mg of sediment was digested in a mixture of concentrated HF, HNO_3 and $HClO_4$ at 90 °C and then dissolved in 1 M HCl. For Fe, Mn, Al and S samples were analyzed using an

inductively coupled plasma optical emission spectrometer (ICP-OES; Perkin Elmer Optima 3000). For Mo, U, Re and V, the same 1 M HCl total digestion extracts were analyzed by ICP-MS. Relative errors were determined using laboratory standards and sample replicates and were generally <5% for the reported elements for the ICP-OES and < 10% for those on the ICP-MS. The limit of detection was 0.2 ppb for Mo, 0.001 ppb for U, 0.0001 ppb for Re and 0.1 ppb for V. Accuracy (recovery) based on average QC yield was between 90 and 99% for all reported elements. The other subsample of the sediment was freeze-dried and the porosity was determined from the weight loss.

Sedimentary organic carbon (C_{org}) and Fe speciation data, including chromium-reducible sulfur (which represents pyrite), for sites 1B, 2, 3, 4, 6B, 8 and 10 were obtained from Kraal et al. (2012). Here, we present additional results for sites 5 and 7. For C_{org} analysis, 200 mg of sediment was decalcified with 1 mol L^{-1} HCl in two steps, (4 h and 12 h), rinsed with ultrapure water and freeze-dried and the C_{org} was measured with a CNS analyzer (Fisons Instruments NA 1500; van Santvoort et al., 2002). For sediment Fe speciation, 50 mg sediment was extracted in the following four steps (Poulton and Canfield, 2005): (1) 1 mol L^{-1} sodium acetate (brought to pH 4.5 with acetic acid, 24 h) to extract carbonate-associated Fe, (2) 1 mol L^{-1} hydroxyl-amine-HCl in 25% v.v. acetic acid (48 h) to extract Fe in amorphous oxides (3) 50 g L^{-1} sodium dithionite buffered to pH 4.8 with 0.35 mol L^{-1} acetic acid/0.2 mol L^{-1} sodium citrate (2 h) to extract Fe in crystalline oxides, (4) 0.2 mol L^{-1} ammonium oxalate/0.17 mol L^{-1} oxalic acid (6 h) to extract Fe in recalcitrant oxides such as magnetite. Chromium-reducible sulfur (CRS) was determined using the chromous chloride distillation method (Canfield et al., 1986) and the associated Fe fraction was calculated assuming the stoichiometry of pyrite.

2.4. Flux calculations

Diffusive fluxes of Mn, Fe, Mo and U across the sediment-water interface were calculated using Fick's first law of diffusion:

$$J = -\phi D_s \frac{dC}{dz}$$

where the diffusive flux is represented by J, the sediment porosity by ϕ, and the sediment diffusion coefficient by D_s and and dC/dz is the concentration gradient between the top layer of the sediment and the bottom water. The D_s was calculated from the molecular diffusion in seawater (for Mn^{2+}, Fe^{2+} and MoO_4^{2-}) corrected for the ambient tortuosity, pressure, temperature and salinity at each site using the R package marelac (Soetaert et al., 2010), which implements the constitutive relations listed in Boudreau (1997). We used the diffusion coefficient of MoO_4^{2-} for U, following Morford et al. (2009), because this captures the transport of uranyl-carbonate complexes, the dominant form of U in seawater. The downward pore water flux of U into the zone of U sequestration was calculated from the concentration gradient of U in the sediment pore water to the depth where U concentrations stabilize. This U flux is referred to as 'deep U flux'.

3. Results

3.1. Pore water

Nitrate was present in the bottom water at all sites (~32 to 40 μmol L^{-1}; Fig. 2). The penetration of NO_3^- into the sediment was lowest at the two OMZ sites 1B and 2 and generally increased with water depth. Pore water Mn concentrations were low (<6 μmol L^{-1}) at the OMZ sites. At the deeper sites, in contrast, Mn increased at depths in the sediment where NO_3^- was depleted (to values up to ~90 μmol L^{-1}). Distinct maxima in pore water Fe concentrations (up to ~100 μmol L^{-1}) were observed at the two OMZ sites 1B and 2. Trends in pore water Fe were comparable to those for Mn at the deeper sites, with the increase in dissolved Fe starting a few centimeters below the increase in Mn. Concentrations of SO_4^{2-} showed little change with depth in the sediment, while pore water H_2S concentrations were mostly at or below the detection limit (see supplementary material). Concentrations of ammonium were low (< 80 μmol L^{-1}) at all sites, with concentrations typically increasing with sediment depth (see supplementary material). Maximum concentrations decreased with increasing water depth. Subsurface peaks of ammonium at sites 6 to 10 are likely a sampling artefact (Grandel et al., 2000; Kraal et al., 2012).

A subsurface peak in dissolved Mo was observed at all sites, except site 1B. A relatively constant background of pore water Mo (~150 nmol L^{-1}) was found at all sites. Dissolved U concentrations in the pore water decreased with depth in the sediment at all sites, generally followed by near constant concentrations below ~10 to 15 cm. Pore water Re ranged mostly between 0.05 and 0.1 nmol L^{-1} at sites 1B, 2 and 3. Pore water V was very low or below detection at sites 1B to 6. At sites 7 to 10, in contrast, a large subsurface peak in pore water V was observed (with values up to ~1000 nmol L^{-1}).

3.2. Calculated diffusive fluxes of (trace) metals

Rates of sediment-water exchange of Mn and Fe, as calculated from the concentration gradients between the bottom water and pore water (Table 2), were quite variable. While an efflux of Mn was calculated for sites1B and 2, a near zero flux was observed at the other sites. For Fe, the calculations suggest a small influx of Fe at 5 out of the 10 sites. Estimated fluxes of Mo and U were also very low, although the results do suggest an efflux of Mo at most sites. The U flux was more variable. The downward deep U fluxes from the surface sediment to the depth of U sequestration ranged from 0.06 to 0.23 nmol cm^{-2} yr^{-1} and were highest at sites 1B and 2.

3.3. Solid phase

Sedimentary C_{org} (Fig. 3) decreased with increasing water depth from ~7 wt% at site 1B to <1 wt% at site 10. Trends in absolute sediment trace metal contents and values normalized over aluminum were generally similar, implying that the trace metal records are not strongly influenced by variable terrigenous detrital inputs (e.g. van der Weijden, 2002).

Sedimentary Mn contents were low (~0.02 wt%) and showed little change with depth at sites 1B and 2. From site 3 downwards, however, surface sediments were enriched in Mn. The magnitude of the Mn enrichments, both with respect to Mn contents (which ranged up to 1 wt%) and the down-core extent of the enrichment, increased with water depth. Sedimentary Fe contents ranged between ~1.5 and 3 wt% but there was no clear trend with water depth and, at most sites, only a small decrease with depth in the sediment was observed. A distinct subsurface enrichment in Fe was observed in the upper 10 cm of Site 1B.

Molybdenum contents at depth in the sediment varied strongly between sites. While for site 1B Mo contents ranged between 2 and 4 ppm, for the other sites Mo contents below the surface sediment were generally <1 ppm. At sites 3 to 10 strong enrichments in surface sediment Mo were observed that mostly tracked Mn contents. Sedimentary U contents were generally relatively constant (< 2 ppm) in the upper ~10 cm of the sediment and then increased with sediment depth at all sites. Sedimentary Re increased with depth at all sites, with the largest enrichment at site 1B. Sedimentary V contents were also highest at site 1B and showed only minor changes change with water or sediment depth.

3.4. Sediment Fe-speciation and total S

Total Fe (Fe_{total}), highly reactive Fe (Fe_{HR}) and Fe oxide (Feox; determined as the sum of the Fe extracted in step 2 and 3 of the extraction) contents generally showed similar trends with depth in the

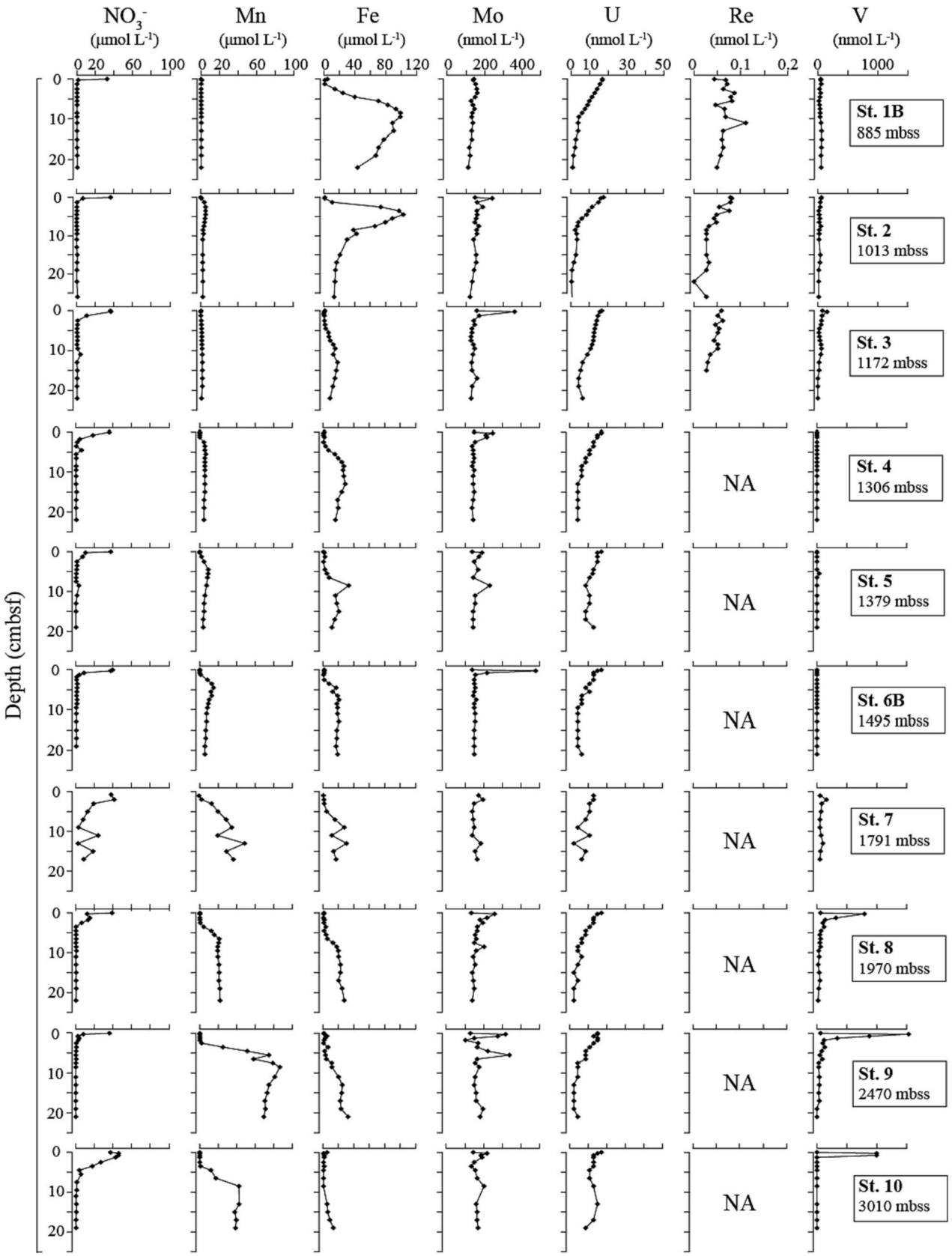

Fig. 2. Pore water depth profiles of NO_3^-, Mn, Fe, Mo, U, Re and V, for the ten study sites along the depth transect at Murray Ridge, northern Arabian Sea. The upper data point indicates the bottom water concentration. Cmbsf = centimeters below the seafloor. NA = not available.

Table 2
Calculated diffusive fluxes of Mn, Fe, Mo and U across the sediment-water interface and, for U, the downward flux into the zone of sedimentary sequestration for sites 1B to 10 (referred to as 'deep U flux'; with the relevant depth intervals used in the calculations indicated between brackets). Negative numbers refer to an influx, positive numbers refer to an efflux. Cmbsf = centimeters below the seafloor.

Site	Mn (μmol cm^{-2} yr^{-1})	Fe (μmol cm^{-2} yr^{-1})	Mo (nmol cm^{-2} yr^{-1})	U (nmol cm^{-2} yr^{-1})	deep U flux (nmol cm^{-2} yr^{-1})
1B	0.41	−1.52	0	−0.01	−0.22 (1.25–9.5 cmbsf)
2	0.30	−0.10	0.05	−0.74	−0.23 (0.25–7.5 cmbsf)
3	−0.09	−0.16	0.10	−0.49	−0.06 (0.25–9.5 cmbsf)
4	0.01	−0.31	0.05	0.01	−0.13 (1.25–8.5 cmbsf)
5	−0.02	0.28	0.02	−0.89	−0.10 (2.5–8.5 cmbsf)
6B	−0.02	0.00	0.14	−0.90	−0.15 (2.5–6.5 cmbsf)
7	0.01	0.20	0.14	0.02	−0.15 (1.0–7.0 cmbsf)
8	0.01	−0.18	0.06	−1.03	−0.13 (2.5–8.5 cmbsf)
9	0.03	0.30	0.09	0	−0.15 (1.75–8.5 cmbsf)
10	0	−1.50	0.03	−0.94	0 (–)

sediment, pointing towards a dominant role for Fe oxides in the sedimentary Fe cycling at these sites. This is confirmed by the pyrite analysis, which indicated that there was appreciable pyrite only at sites 1B and 2. At most sites, only little Fe was dissolved in the extraction steps targeting Fe carbonates (step 1) and magnetite and other crystalline Fe oxides (step 4) (see supplementary material). Sediment S contents ranged between 0.1 and 0.6 wt%, with the highest values at the OMZ site 1B (see supplementary material).

4. Discussion

4.1. Impact of the OMZ on sediment Mn and Fe redox chemistry

Pore water profiles of dissolved NO_3^-, Mn and Fe along the water depth transect (Fig. 2) reflect the typical redox zonation upon degradation of organic matter in sediments (Froelich et al., 1979). This implies that first Mn and then Fe emerge in the pore water in dissolved form at depths where NO_3^- is depleted. The differences in pore water Mn and Fe between sites are primarily the result of variations in the input of organic matter and bottom water oxygen that depend on water depth as detailed below.

At the locations within the core of the OMZ (sites 1B and 2) the relatively high input of organic matter and low bottom water oxygen (Table 1) promote reductive dissolution of Mn oxides in the water column and at the sediment-water interface, with subsequent return of the Mn to the OMZ waters in dissolved form (Table 2). This explains why sediments in the area are nearly devoid of solid phase Mn (Fig. 3), in line with previous observations that Arabian Sea OMZ waters are enriched in dissolved Mn (Lewis and Luther, 2000). While dissolved Mn decreases in the waters below the OMZ, particulate Mn concentrations increase (Nair et al., 1999; Lewis and Luther, 2000), pointing towards oxidation of dissolved Mn to Mn oxides. The settling of these Mn oxides explain the Mn enrichments observed in sediments below the OMZ (Fig. 4). Similar enrichments have also been observed near the Pakistan margin (Schenau et al., 2002; Law et al., 2009) and have been attributed to redox-driven redistribution of Mn. When including a sediment component, such Mn redistribution is referred to as "Mn shuttling" (Lyons and Severmann, 2006; Lenstra et al., 2020). Manganese shuttling also occurs in the Peruvian and Chilean OMZs (e.g. Böning et al., 2005; Scholz et al., 2011). However, in these regions, the zone of sediment Mn depletion extends into areas with well-oxygenated bottom waters below the OMZ (Scholz, 2018), whereas in the Arabian Sea, Mn oxides are present in sediments below the OMZ (Fig. 3). This may be explained by a generally higher input of organic matter - a key reductant for Mn oxides – at the same bottom water oxygen concentration in the Eastern Tropical South Pacific when compared to the Arabian Sea, which is reflected in generally higher sediment C_{org} values in the former region (e.g. Böning et al., 2004).

The sedimentary dynamics of Fe in and below the Arabian Sea OMZ differ from those of Mn. Iron oxides are abundant in the OMZ sediments (Fig. 4). The maxima in pore water Fe (Fig. 3), point towards active diagenetic Fe cycling at all sites although pyrite formation is generally limited. The peak in pyrite at depth at site 2 is a non-steady state feature, and likely does not represent ongoing diagenesis (Kraal et al., 2012). There is no indication for substantial benthic release of Fe (Table 2) and cycling of Fe thus is mostly restricted to the sediment. This precludes a major role for Fe shuttling, despite the abundant presence of Fe in the OMZ sediments (Fig. 4). The lack of a trend in the sulfate profiles (see supplementary material) and limited Fe-S accumulation suggest low rates of sulfate reduction.

These results for the Arabian Sea OMZ contrast with the sedimentary Fe cycling in and below the OMZ as reported, for example, for the Peru margin. In the latter region, pyrite is the principal burial phase for reactive Fe and net downward supply of reactive Fe from the margins to the deep sea occurs through Fe shuttling driven by benthic Fe release from OMZ sediments (e.g. Scholz et al., 2014a; 2014b; Scholz, 2018). Again, a higher input of reactive organic matter linked to a higher primary productivity and more intense anoxia in bottom waters in the Peru OMZ when compared to the Arabian Sea sediments can explain these results. These differences could possibly be amplified by lateral input of organic matter to Peru OMZ sediments from the adjacent shelf, a process which is absent on Murray Ridge because of its isolated position. Indeed, reactive transport modeling suggests that anaerobic degradation pathways of organic matter are quantitatively more important in Peru margin versus Arabian Sea sediments (Bohlen et al., 2011; Kraal et al., 2012). Water depth could also play a role in the case of the Murray Ridge since we do not capture OMZ sites shallower than 885 m while most studies for other regions cover the full depth range of the OMZ (e.g. Scholz et al., 2014b; Callbeck et al., 2021). A deeper site implies that a larger proportion of the sinking reactive organic matter will have been degraded prior to reaching the sediment, even when considering less decay because of the anoxic water column (Keil et al., 2016; Nierop et al., 2017). However, sediment Fe-S data from the Oman (Passier et al., 1997) and Pakistan margin (Law et al., 2009) point towards relatively low rates of sulfate reduction and pyrite formation in OMZ sediments at shallower water depths (~450 and 300 m, respectively), suggesting that water depth is not the only control. Further work on sedimentary Mn and Fe cycling is clearly needed at other OMZ sites in the Arabian Sea, e.g. off the west coast of India where rates of organic matter input to the sediment appear to be higher (Fernandes et al., 2018).

The effect of the presence of the OMZ on Mn and Fe burial at Murray Ridge can be visualized by comparing the average sediment Mn/Al and Fe/Al ratios per site (Fig. 5). The results show depletion of sediment Mn at OMZ sites, whereas notably high Mn is observed at the oxic sites 9 and 10 below the OMZ, illustrating the role of Mn shuttling. Only Mn that is converted from Mn oxide to Mn carbonate will be permanently buried in the sediment (e.g. Schenau et al., 2002). In accordance with limited Fe shuttling, we find no clear trend in sedimentary Fe (Fig. 5) or highly reactive Fe/total Fe (Fig. 4 and see supplementary material), apart from the higher values at the shallowest OMZ site 1B. In the case of the OMZ at Murray Ridge, the sediments are not reducing enough to allow for substantial redistribution of Fe along the redox transect. Based on the highly reactive Fe to total Fe ratios alone, site 1B would classify as anoxic/ferruginous, whereas sites 2 to 10 would classify as oxic (Raiswell et al., 2018; Hardisty et al., 2018). Our results confirm earlier work

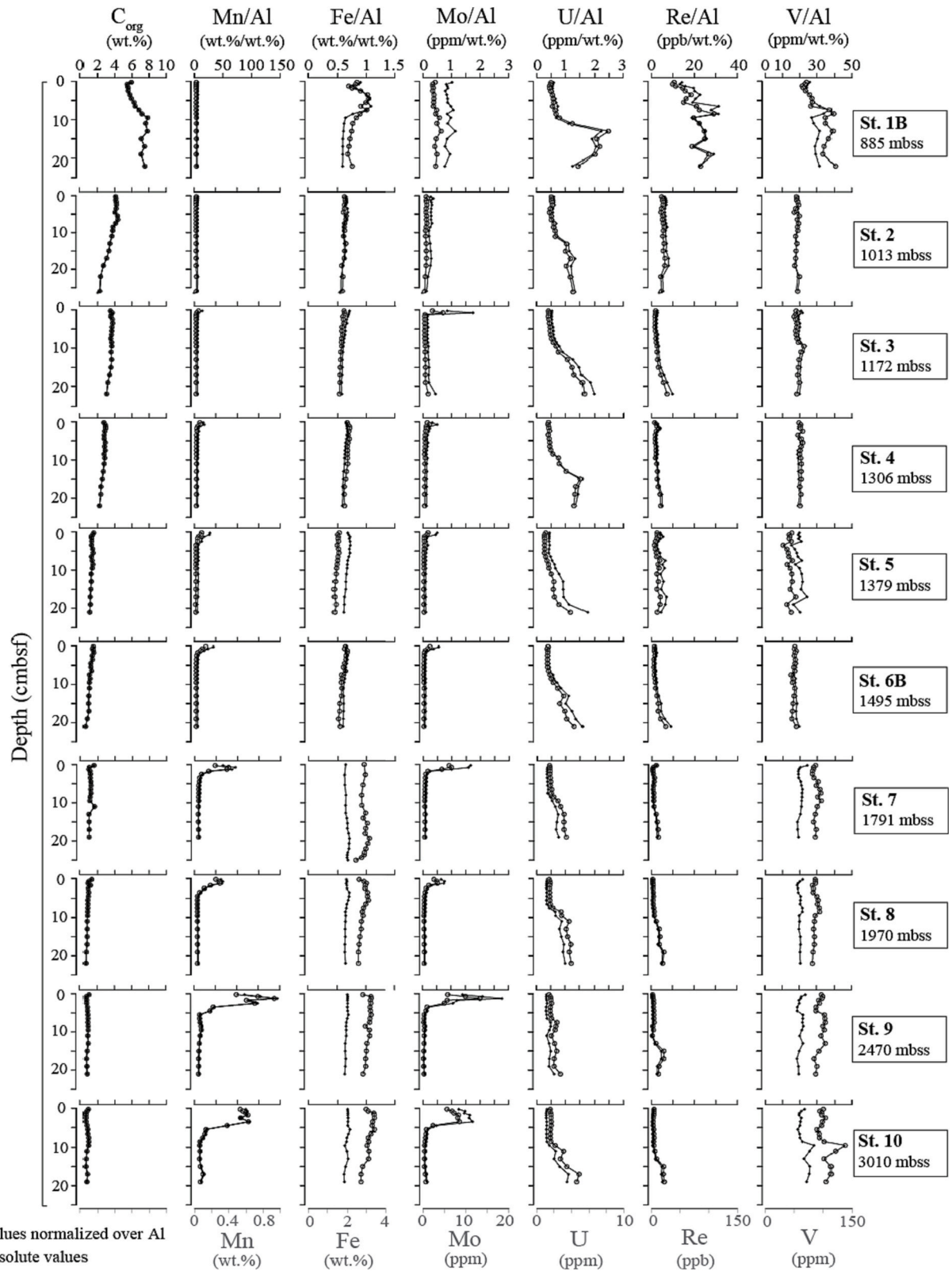

Fig. 3. Solid phase depth profiles of C_{org}, Mn, Mn/Al, Fe, Fe/Al, Mo, Mo/Al, U, U/Al, Re, Re/Al, V and V/Al, for the 10 sites along the depth transect on Murray Ridge, northern Arabian Sea. Absolute values for the trace metals are in grey, values normalized over aluminum in black. Cmbsf = centimeters below the seafloor.

showing that the dynamics of Fe in OMZs are complex, that anoxia does not necessarily lead to Fe enrichments in the form of pyrite and that Fe proxies should be used with caution in such settings (Scholz, 2018).

4.2. Trace metal enrichments: sources of the metals

Average Mo/Al, U/Al, Re/Al ratios (Fig. 5) for all sites show again that Mo, U and Re are enriched in the sediment at the OMZ site 1B when

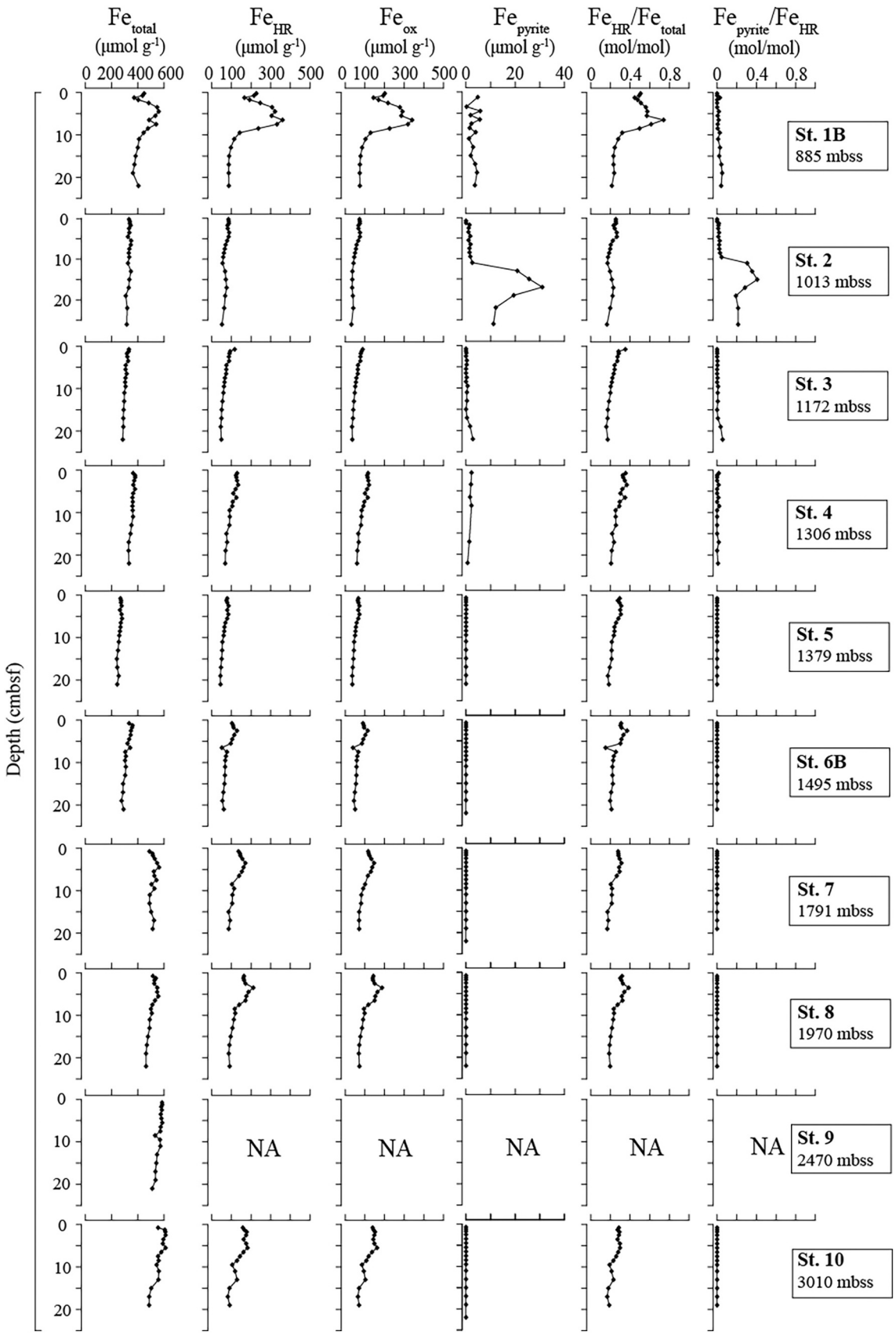

Fig. 4. Depth profiles of various sediment Fe-forms: total Fe (Fe_{total}), highly reactive Fe (Fe_{HR}, the sum of all the fractions obtained from the sequential Fe extraction and Fe in pyrite based on CRS; Kraal et al., 2012), Fe in pyrite (Fe_{pyrite}), Fe-oxides (Fe_{ox}), Fe_{HR}/Fe_{total} and Fe_{pyrite}/Fe_{HR}. Cmbsf = centimeters below the seafloor. NA = not available.

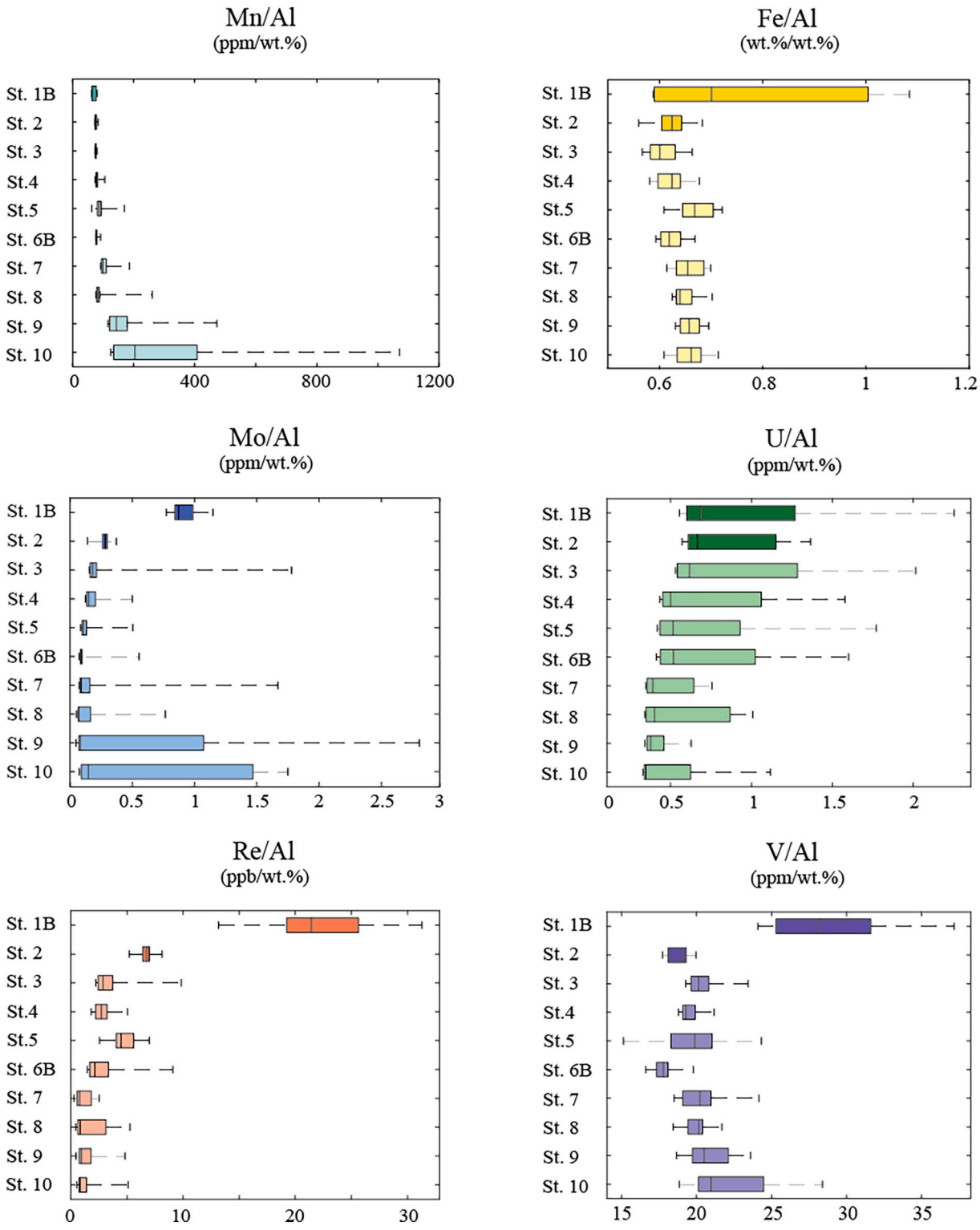

Fig. 5. Box and whisker plots with average sedimentary trace metal concentrations normalized over aluminum for all sites. Boxes represent the 1st and 3rd quartile, separated by the median; whiskers indicate minimum and maximum values.

compared to most other sites. The decrease in concentraton with increasing water depth implies that these trace metals capture the general trend in bottom water oxygen concentrations, especially at sites 1B to 7 (Table 1; Fig. 5). For Mo, the enrichment in the deeper oxic stations 9 and 10 is the result of the association of Mo with Mn-oxides, as further discussed below. Vanadium, in contrast, is only enriched at the OMZ site 1B. Below, we discuss the potential sources of the trace metals, i.e. the role of deposition of trace metals associated with organic matter (e.g. Algeo and Lyons, 2006; Tribovillard et al., 2006) or Mn and Fe oxides (e.g. Bertine and Turekian, 1973; Crusius et al., 1996) and the role of diffusion from the bottom water (e.g. Scholz et al., 2011).

For Mo, diffusion from the water column cannot be important because the flux is mostly directed out of the sediment (Table 2). Instead, maxima in pore water Mo observed near the sediment-water

interface at all sites point towards release of Mo from a particulate phase. Organic matter is an unlikely source of this Mo. Molybdenum contents of marine phytoplankton are orders of magnitude too low. For example, an average Mo/C_{org} ratio of 0.21 μmol/mol (range of 0.05 to 0.72 μmol/mol) was reported for phytoplankton from key marine phyla (Ho et al., 2003), while sediments deposited under low-oxygen conditions typically have a Mo/C_{org} ratio >10 μmol/mol (Helz and Vorlicek, 2019). Scavenging of Mo by sulfide associated with sinking organic matter (Algeo and Lyons, 2006; Dahl and Wirth, 2017; Helz and Vorlicek, 2019) and subsequent release of Mo in the surface sediment also appears unlikely because of the lack of sufficiently reducing conditions in the Arabian Sea OMZ. The capture of Mo by extracellular mucilage released from algae (*Phaeocystis*), as reported for coastal waters along the North Sea coast (Dellwig et al., 2007), requires a type of algal species that is not present in open ocean environments. Hence, the most likely source of Mo here is the deposition of metal oxides. Based on the cycling of Mn and Fe described in Section 4.1, Mn oxides are the most likely carrier of Mo to the sediment along the transect, with reductive dissolution of Mn oxides (or desorption of Mo) explaining the release of Mo to the pore waters (Shimmield and Price, 1986; Zheng et al., 2000). Part of the Mo directly escapes to the overlying water through diffusion (Table 2) while part of the Mo diffuses downward to be sequestered as solid phase Mo. Because there is no corresponding peak in dissolved Mn at the same depth as Mo in the pore water at the sites below the OMZ, Mn released through reductive dissolution must be directly bound in the sediment, possibly through sorption onto Mn oxides (Shimmield and Price, 1986) or precipitation as Mn carbonate (e.g. Schenau et al., 2002).

To obtain further insight into the association of Mo with other sediment components, we plotted the Mo contents as a function of the C_{org} and total Mn content for all sites (Fig. 6). From these plots, two groups of data points emerge that correspond to the locations of the sites along the redox transect and reflect differences in Mo sequestration. At sites 1B to 4, we find a positive correlation between Mo and C_{org} contents (Fig. 6a) but no link between Mo and Mn (Fig. 6b). These sediments are slightly enriched in S relative to the other sites along the transect (see supplementary material; Kraal et al., 2012) and low rates of sulfate reduction linked to organic matter degradation likely explain the sequestration of Mo (also see Helz and Vorlicek, 2019). A ratio of ~0.6 ppm Mo/wt% C_{org} is obtained from the slope of the dataset for sites 1B to 4, which is much lower than observed in sediments of anoxic basins (range of 4.5 to 45 ppm/wt%; Algeo and Lyons, 2006). We see no relationship between Mo and C_{org} at the other sites (Fig. 6a) but for sites 5 to 10, a correlation between Mo and Mn is observed instead (Fig. 6b). The slope of 11 ppm Mo/wt% Mn for these sites is roughly half the value typically observed for Mn oxides in marine sediments (~20 ppm Mo/wt % Mn; Shimmield and Price, 1986). This difference could be explained by the presence of Mn carbonates (Schenau et al., 2002), which, in contrast to Mn oxides, do not adsorb Mo.

Pore water profiles of U point towards an influx of U from the overlying water at several sites and downward diffusion and removal of dissolved U at sediment depths of 10–15 cm in the zone of Fe oxide reduction at all sites (Fig. 2). The removal of U is likely the result of reduction of U(VI) to U(IV) in pore water and subsequent formation of UO_2 linked to microbial activity (e.g. Klinkhammer and Palmer, 1991; McManus et al., 2005, 2006; Scholz, 2018). Hence, the sequestration of U is not only linked to bottom water oxygen concentrations, but also to other factors such as the rate of input of organic matter and Fe oxides. Our results indicate that the changes in these factors are not large enough to lead to major changes in U sequestration in the sediments along the water depth transect below the OMZ. If we assume that all downward diffusing U is fixed in the sediment, rates of authigenic U formation would range from 0.06 to 0.22 nmol cm^{-2} yr^{-1} (Table 2). These values fall within the range reported for downward pore water U fluxes for sediments from the California margin (0.06 to 0.53 nmol cm^{-2} yr^{-1}; McManus et al., 2006). The removal of U from the pore water leads to an enrichment in U in the solid phase at all sites (Figs. 2 and 3). The rates of sediment accumulation are not well-constrained at our sites, despite ^{210}Pb and ^{14}C dating (Koho et al., 2013). Therefore, we cannot accurately calculate rates of U accumulation based on the sediment profiles. If we nevertheless take the range of mass accumulation rates from Koho et al. (2013) and multiply them with the maximum U concentrations at depth at our sites, we obtain a range of U accumulation fluxes of 0.04 to 0.24 nmol cm^{-2} y^{-1} which, although not always matching the diffusive influxes at each site, are within the same range (Table 2; see supplementary material).

Rhenium is enriched at depth in the sediment at all sites (Fig. 3), with Re contents generally decreasing with increased water depth (Fig. 5) and bottom water oxygen. Such enrichments of Re in sediments are thought

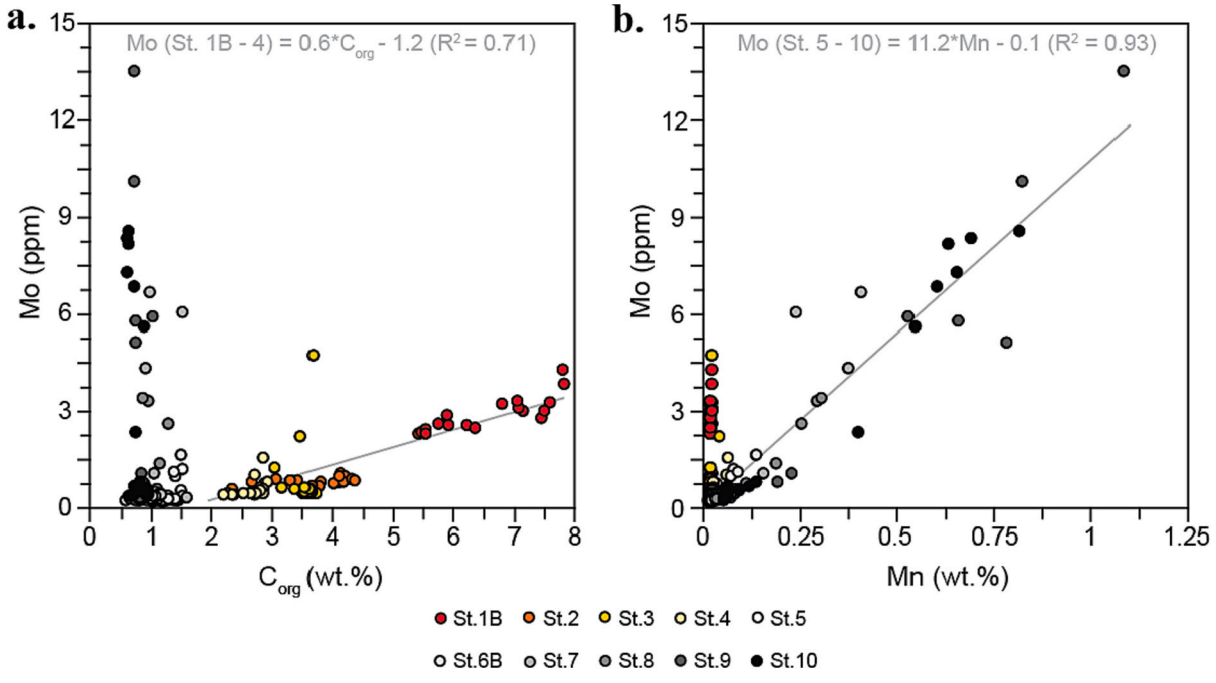

Fig. 6. Relationship between sediment Mo (in ppm) and (a.) C_{org} (wt%) and (b.) Mn (wt%) in the sediment at sites 1B to 10.

to be the result of precipitation of Re from pore waters under reducing conditions (Crusius et al., 1996; Morford et al., 2012). The downward flux of dissolved Re in the pore water at sites 1B to 3 supports such a mechanism (Fig. 2). We note, however, that pore water concentrations of Re in the surface sediment are higher than in the bottom water. This might reflect release of Re from a particulate source that has been reported for other regions but as yet still needs to be characterized (Helz, 2022). Vanadium is only enriched in the sediment at one of the OMZ sites (site 1B; Figs. 4 and 5). The absence of a clear trend in sedimentary V as a function of bottom water oxygen could be related to the low rates

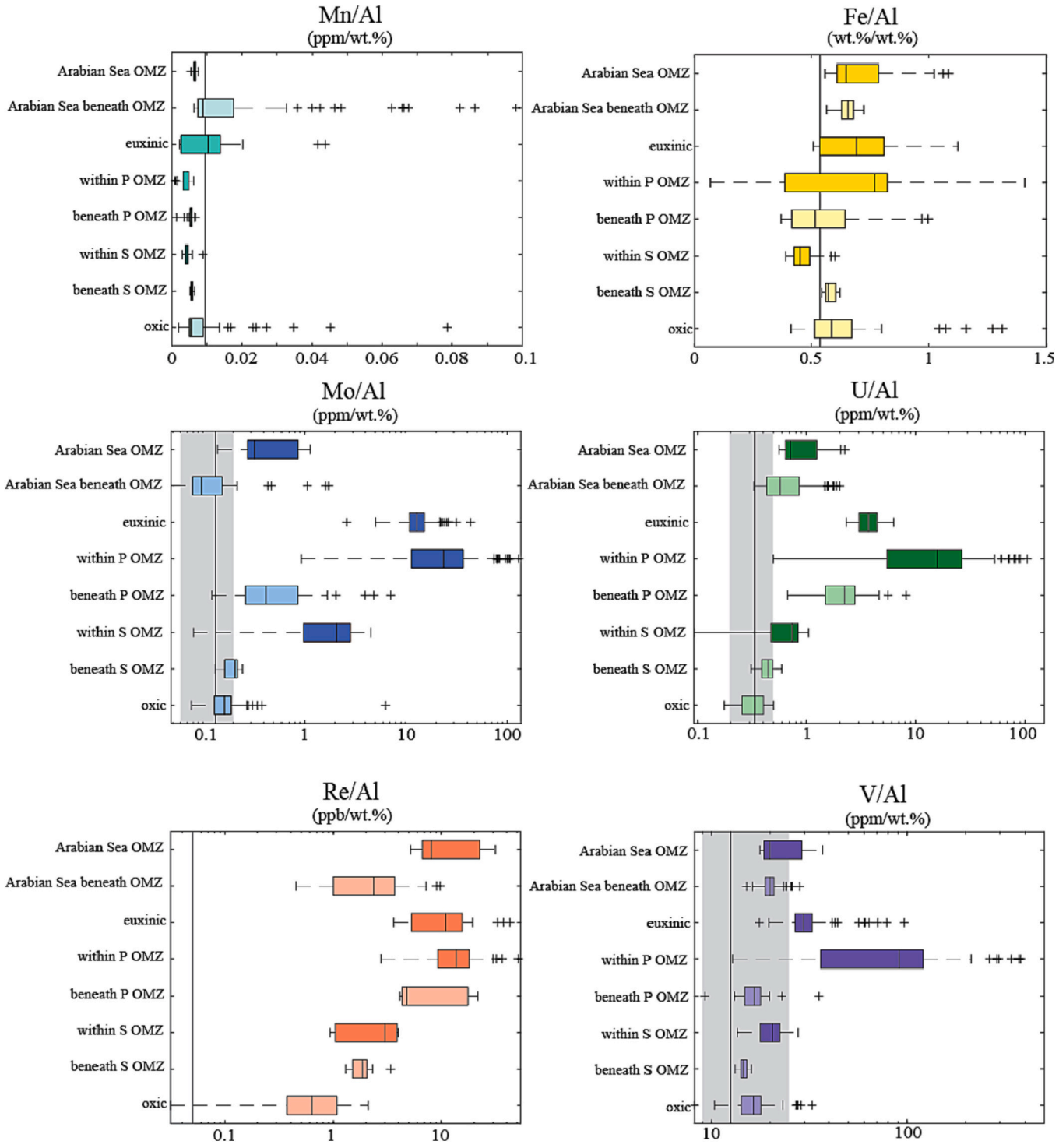

Fig. 7. Box and whisker plots of sediment Mn, Fe, Mo, U, Re and V contents normalized over Al for a range of modern marine depositional environments on a $\log_{10}$ scale based on the approach by Bennett and Canfield (2020). Our data are presented as Arabian Sea OMZ (sites 1B and 2) and Arabian Sea beneath OMZ (sites 3 to 10). The other data are presented in six groups: euxinic systems; within and beneath a perennial OMZ, (i.e. year-round anoxic conditions; P-OMZ); within and beneath a seasonal OMZ, (i.e. seasonally anoxic conditions; S-OMZ) and oxic systems. Boxes represent the interquartile range, the whiskers represent the 5th and the 95th percentiles, the vertical lines represent the mean values. Data exceeding the 5th and 95th percentiles are indicated as a plus (+). The crustal average (Rudnick and Gao, 2013) is shown as a grey solid line with two standard deviations represented by the grey shading, except for Mn, Fe and Re, where the grey line represents an estimate of the crustal average (Li and Schoonmaker, 2003; Rudnick and Gao, 2013).

of sulfate reduction in the Arabian Sea sediments, since the presence of free sulfide can enhance formation of authigenic V (Morford and Emerson, 1999). At many of the sites, pore water V concentrations are too low to provide insight into the processes supplying V and the depth of its sequestration (Fig. 2). At sites 7 to 10, however, a sharp peak in pore water V is observed near the sediment-water interface. Potential sources of V include release from organic matter upon its degradation or from metal oxides upon reductive dissolution (Morford et al., 2005; Scholz et al., 2011). The enrichment in total V in the surface sediment at these same sites points towards an inorganic source, however. Given the strong shuttling of Mn in this system (Section 4.1), we suggest that Mn oxides are a major carrier of V to these sediments, although we cannot exclude an additional role for Fe oxides, supplied, for example, from dust (Kraal et al., 2012).

In summary, our results suggest a role for metal oxides as a source of both Mo and V to sediments in and below the Arabian Sea OMZ. This is in line with work for other OMZs, although the role of Fe and Mn oxides as a source of Mo may vary (e.g. Scholz et al., 2017; Scholz, 2018; Ho et al., 2018; Eroglu et al., 2020; He et al., 2021). Along the Peru margin, for example, Fe oxides were found to dominate over Mn oxides as a source of Mo in the OMZ (Eroglu et al., 2020). Our results for U and Re are also in accordance with those reported for other OMZs (e.g. Scholz, 2018), with authigenic U and Re fixation after downward diffusion from surface sediments to greater depths. Whether release from particles contributes to some of the dissolved U and Re in the surface sediment can not be determined from our data.

4.3. Trace metals as a redox proxy

Sediment contents of Mo, U and Re along our transect capture the general trend in bottom water oxygen concentrations, whereas V does not (Table 1; Fig. 5). To further evaluate the role of these metals as redox proxies, we compare the sediment contents for our study sites in the Arabian Sea to those observed in other systems and to key thresholds for perennial OMZs as proposed in the literature. We include Mn and Fe in our comparison, given the role of Mn and Fe oxides as a carrier of trace metals.

We make use of the data compilation of Bennett and Canfield (2020), which includes trace metal data for sediments from within and below perennial and seasonal OMZs (excluding the Arabian Sea), besides oxic continental margin and euxinic basin settings (Fig. 7). We include estimates of the crustal average (Rudnick and Gao, 2013) in the figure to emphasize where values are enriched. The Mn/Al data show that sediments in and below the Arabian Sea OMZ (defined here as sites 1B and 2 versus 3 to 10) are depleted in Mn when compared to the crustal average but enriched relative to other OMZs. This is in line with the less reducing nature of the OMZ sediments in the Arabian Sea when compared to the other OMZs and the shuttling of Mn discussed above. The lack of clear trends in Fe/Al confirms the complex dynamics between Fe cycling and bottom water redox conditions in OMZs, as discussed, for example, by Scholz (2018).

Sediments beneath the Arabian Sea OMZ are characterized by Mo/Al values similar to those for the continental crust (Li and Schoonmaker, 2003; Rudnick and Gao, 2013). Sediments in the Arabian Sea OMZ are enriched in Mo relative to crustal values but values lie below those for euxinic systems and the seasonal and perennial OMZs. This illustrates that, in the Arabian Sea, sediment Mo contents respond to bottom water anoxia even though conditions are much less reducing than in other perennial OMZs. This also highlights that the threshold of 5 ppm/wt% for Mo/Al proposed for perennial OMZs (Bennett and Canfield, 2020) is too high to detect perennial OMZs that are less reducing than those that the classification is based on, such as the Arabian Sea OMZ studied here.

For U/Al, the picture is slightly different: sediments in and below the Arabian Sea OMZ are enriched in U relative to the crustal average, with highest U/Al values in the OMZ sediments. While U/Al values for the Arabian Sea OMZ lie below those for euxinic systems and perennial OMZs, they are elevated when compared to seasonal OMZs. Again, however, the U/Al values lie below the threshold defined for perennial OMZs, which in this case is also 5 ppm/wt%.

Values of Re/Al are above crustal averages in all OMZ regions, and again, a distinct difference between sediments in and below the Arabian Sea OMZ is observed with the highest values in the OMZ sediments. Interestingly, values of Re/Al in Arabian Sea OMZ sediments are comparable to values for euxinic systems and for sediments in and below other perennial OMZs, whereas the sediments beneath the Arabian Sea OMZ have Re/Al values comparable to those in OMZs.

The V/Al ratios of the sediments in and below the Arabian Sea OMZ mostly fall within the range of values for the average continental crust, as do the values in and below seasonal OMZs and below other perennial OMZs. However, V/Al values in OMZs are generally higher than below the OMZ. Strong enrichments in V values are only observed in sediments of other perennial OMZs. Bennett and Canfield (2020) argued that a threshold of 23 ppm/wt% for V/Al could be used to distinguish sediments located in and below perennial OMZs, with values >46 ppm/wt% providing strong evidence for a location in the anoxic core. Our results show that V/Al in our Arabian Sea OMZ sediments only partly lie above the 23 ppm/wt% threshold.

To explore the potential role of regional differences in trace metal sequestration in sediments in the Arabian Sea OMZ, we compared our results to data for a sediment core from the OMZ along the Oman margin (Morford and Emerson, 1999) and to surface sediments from three sites with bottom water oxygen concentrations ranging from 1.4 to 2.2 μmol L^{-1} from the margin along the western coast of India (Kessarkar et al., 2022; Table 3). The Mo/Al and U/Al data for these sites are also lower than the threshold of 5 ppm/wt% for a perennial OMZ (Bennett and Canfield, 2020). Values of V/Al mostly lie close to the threshold of 23 ppm/wt%, however.

In summary, while Mo, U, and Re are suitable redox proxies in Arabian Sea sediments, V is only an indicator for the most intense section of the OMZ sampled here. Furthermore, values of Mo/Al and U/Al in the Arabian Sea OMZ sediments studied so far are lower than the thresholds suggested for perennial OMZs (Bennett and Canfield, 2020). We attribute this to a generally lower productivity in the regions of the Arabian Sea studied here and, as a consequence, less reducing conditions in the sediments. Further work in other areas in the Arabian Sea is needed to create a complete picture for the region. Our results imply that

Table 3
Average trace metal contents normalized over Al for Arabian Sea OMZ sediments from Murray Ridge for sites 1B and 2 (this study), for an OMZ site along the Oman margin (Oman TN047–20; Morford and Emerson, 1999), for three OMZ sites along the Western margin of India (W-India G1–3; Kessarkar et al., 2022) and for long core PC463 at Murray Ridge capturing the period from 15 to 200 ka (van der Weijden et al., 2006; based on the supplementary data file). Minimum and maximum values are given between brackets. Mbss = meters below sea surface. NA = not available.

Parameter	Murray ridge Site1B	Murray ridge Site 2	Oman TN047–20	W-India G1–3	Murray ridge PC463
Water depth (mbss)	885	1013	806	197, 384, 648	970
Mo/Al (ppm/wt %)	0.9 (0.8–1.1)	0.3 (0.1–0.4)	2.4 (1.9–3.6)	0.4 (0.3–0.5)	1.7 (0.3–5)
U/Al (ppm/wt %)	1.0 (0.6–2.3)	0.8 (0.6–1.4)	2.5 (2.0–2.9)	2.4 (0.9–4.8)	1.2 (0.5–3.4)
Re/Al (ppb/wt %)	22 (13–32)	7 (5–8)	18 (17–19)	NA	7 (1–22)
V/Al (ppm/wt %)	29 (24–37)	19 (18–20)	25 (23–27)	22 (19–27)	20 (17–31)

perennial OMZs, with characteristics like those of the parts of the Arabian Sea included here, could be overlooked when only using the thresholds for Mo/Al and U/Al for their detection in the geological record.

4.4. Redox changes in the Arabian Sea over the past ~200 kyrs

The intensity and vertical extent of the Arabian Sea OMZ has varied on millennial time scales due to changes in monsoonal activity (Schulz et al., 1998; Schulte et al., 1999; Reichart et al., 1998). Such variations have been shown to be reflected in sedimentary trace metal records for Arabian Sea sediments on Murray Ridge from 15 to 200 ka (van der Weijden et al., 2006), Since our study sites are located along the same ridge, the trace metal data for the OMZ can be compared and used to assess potential differences between the intensity of the present-day and past OMZ.

We focus here on Mo/Al, U/Al, Re/Al and V/Al records for a site in the OMZ (PC463) with a water depth that is close to that of our sites 1B and 2 and compare average values of sediment contents including the range (i.e. minima and maxima; Table 3). As discussed by van der Weijden et al. (2006), the record for PC463 shows distinct variations with maximum trace metal values in sediments during periods of enhanced productivity and intensification of the OMZ. For Mo/Al and U/Al, modern day values mostly lie within the lower part of the range observed in PC463, indicating that the OMZ was more intense in the past than it is today. Still, based on the values below 5 ppm/wt%, the Arabian Sea OMZ at this water depth was never as reducing as current other perennial OMZs (see Section 4.3; Fig. 7). Values for Re/Al and V/Al at sites 1B are close to maximum values in the record for PC463, however. Taken together, this suggests differences in the processes contributing to sequestration of Re and V relative to Mo and U in the present-day and past OMZ and/or reflects effects of diagenesis.

Differences in ratios of Re/Mo illustrate this contrast, also when only considering the authigenic component normalized to seawater i.e. ratios of $(Re_{auth}/Mo_{auth})_{sw}$ using methods outlined by Helz (2022), see supplementary material). While an average $(Re_{auth}/Mo_{auth})_{sw}$ ratio of 8 is observed for PC463 (Helz, 2022), we find a value of 34 for our OMZ sites 1B and 2. As discussed by Helz (2022), Arabian Sea sediments have much higher Re/Mo ratios than other upwelling environments. Our work confirms that this is mostly the result of lower sediment Mo contents.

5. Conclusions

Sediment trace metals such as Mo, U, Re and V are frequently used in reconstructions of redox conditions in the past ocean. We combined pore water and sediment analyses for ten sites in and below the Arabian Sea OMZ to assess the likely sources of trace metals in the sediment and their use as a redox proxy. The results suggest that most U enters the sediment through diffusion across the sediment-water interface, while Mo and V are mostly supplied in particulate form, likely mainly associated with Mn oxides. The supply mechanism for Re could involve a particulate form but sequestration likely follows downward diffusion. Sediments of the Arabian Sea OMZ are enriched in Mo, U, Re and V. Changes in Mo, U and Re reflect bottom water oxygen concentrations in and below the Arabian Sea OMZ and hence are suitable redox proxies. In contrast, V does not capture the change in bottom water redox conditions with increasing water depth. Enrichments of Mo, U and V in the regions of the Arabian Sea studied so far are less pronounced than in other perennial OMZs, indicating that care should be taken when using thresholds of trace metal contents to identify such OMZs. Based on a comparison of Mo/Al and U/Al records for the modern and from 15 to 200 ka, we conclude that the Arabian Sea OMZ was periodically more intense than at present.

Declaration of Competing Interest

The authors declare that they have no known competing financial interests or personal relationships that could have appeared to influence the work reported in this paper.

Data availability

Data included in supplementary file

Acknowledgements

We thank the captain and crew of R/V *Pelagia* and the shipboard party and chief scientist (G.J. Reichart) for their contribution to the sampling. We are grateful to H. de Waard for analytical assistance in Utrecht. A. Vollebregt acknowledges funding from the Netherlands Organisation for Scientific Research (NWO) grant "Promotiebeurs voor Leraren" 023.015.001. The research presented in this paper was also financially supported by NWO Vidi grant 864.05.004 and ERC Starting grant 278364 (to C.P. Slomp) and by a grant from the Olaf Schuiling Fund at Utrecht University (to S. Pit). The cruise was funded by NWO grant 817.01.015. This work was carried out under the program of the Netherlands Earth System Science Center (NESSC), financially supported by the Ministry of Education, Culture and Science, grant no. 024.002.001. (OCW). We thank Xinming Chen and two anonymous reviewers for constructive reviews and Karen Johannesson for editorial handling.

Appendix A. Supplementary data

Supplementary data to this article can be found online at https://doi.org/10.1016/j.chemgeo.2022.121300.

References

Acharya, S.S., Panigrahi, M.K., 2016. Eastward shift and maintenance of Arabian Sea oxygen minimum zone: understanding the paradox. Deep Sea Res. Part I Oceanogr. Res. Pap. 115, 240–252.
Algeo, T.J., Li, C., 2020. Redox classification and calibration of redox thresholds in sedimentary systems. Geochim. Cosmochim. Acta 287, 8–26.
Algeo, T.J., Lyons, T., 2006. Mo-total organic carbon covariation in modern anoxic marine environments: Implications for analysis of paleoredox and paleohydrographic conditions. Paleoceanography 21, PA1016.
Algeo, T.J., Tribovillard, N., 2009. Environmental analysis of paleoceanographic systems based on molybdenum-uranium covariation. Chem. Geol. 268, 211–225.
Bennett, W.W., Canfield, D.E., 2020. Redox-sensitive trace metals as paleoredox proxies: a review and analysis of data from modern sediments. Earth Sci. Rev. 204, 103175.
Bertine, K., Turekian, K., 1973. Molybdenum in marine deposits. Geochim. Cosmochim. Acta 37, 1415–1434.
Bohlen, L., Dale, A., Sommer, S., Mosch, T., Hensen, C., Noffke, A., Scholz, F., Wallmann, K., 2011. Benthic nitrogen cycling traversing the Peruvian oxygen minimum zone. Geochim. Cosmochim. Acta 75, 6094–6111.
Böning, P., Brumsack, H.J., Böttcher, M.E., Schnetger, B., Kriete, C., Kallmeyer, J., Borchers, S.L., 2004. Geochemistry of Peruvian near-surface sediments. Geochim. Cosmochim. Acta 68, 4429–4451.
Böning, P., Cuypers, S., Grunwald, M., Schnetger, B., Brumsack, H.J., 2005. Geochemical characteristics of Chilean upwelling sediments at similar to ~ 36°S. Mar. Geol. 220, 1–21.
Boudreau, B.P., 1997. Diagenetic Models and their Implementation. Springer.
Breitburg, D., Levin, L.A., Oschlies, A., Grégoire, M., Chavez, F.P., Conley, D.J., Garçon, V., Gilbert, D., Gutiérrez, D., Isensee, K., Jacinto, G.S., Limburg, K.E., Montes, I., Naqvi, S., Pitcher, G.C., Rabalais, N.N., Roman, M.R., Rose, K.A., Seibel, B.A., Telszewski, M., Zhang, J., 2018. Declining oxygen in the global ocean and coastal waters. Science 359, eaam7240.
Brumsack, H.J., 1989. Geochemistry of recent TOC-rich sediments from the Gulf of California and the Black Sea. Int. J. Earth Sci. 78, 851–882.
Callbeck, C.M., Canfield, D.E., Kuypers, M.M.M., Yilmaz, P., Lavik, G., Thamdrup, B., Schubert, C.J., Bristow, L.A., 2021. Sulfur cycling in oceanic oxygen minimum zones. Limnol. Oceanogr. 66, 2360–2392.
Calvert, S., Pedersen, T., 1993. Geochemistry of recent oxic and anoxic marine sediments: Implications for the geological record. Mar. Geol. 113, 67–88.
Canfield, D., Raiswell, R., Westrich, J., Reaves, C., Berner, R., 1986. The use of chromium reduction in the analysis of reduced inorganic sulfur in sediments and shales. Chem. Geol. 54, 149–155.

Cochran, J.K., Carey, A.E., Sholkovitz, E.R., Surprenant, L.D., 1986. The geochemistry of uranium and thorium in coastal marine sediments and sediment pore waters. Geochim. Cosmochim. Acta 50, 663–680.
Cowie, G.L., Levin, L.A., 2009. Benthic biological and biogeochemical patterns and processes across an oxygen minimum zone (Pakistan margin, NE Arabian Sea). Deep-Sea Res. II 56, 261–270.
Crusius, J., Calvert, S., Pedersen, T., Sage, D., 1996. Rhenium and molybdenum enrichments in sediments as indicators of oxic, suboxic and sulfidic conditions of deposition. Earth Planet. Sci. Lett. 145, 65–78.
Dahl, T.W., Wirth, S.B., 2017. Molybdenum isotope fractionation and speciation in a euxinic lake—Testing ways to discern isotope fractionation processes in a sulfidic setting. Chem. Geol. 460, 84–92.
Dellwig, O., Beck, M., Lemke, A., Lunau, M., Kolditz, K., Schnetger, B., Brumsack, H.J., 2007. Non-conservative behaviour of molybdenum in coastal waters: Coupling geochemical, biological, and sedimentological processes. Geochim. Cosmochim. Acta 71, 2745–2761.
Endrizzi, F., Rao, L., 2014. Chemical speciation of uranium (VI) in marine environments: complexation of calcium and magnesium ions with $[(UO^2)(CO_3)_3]^{4-}$ and the effect on the extraction of uranium from seawater. Chem Eur J 20 (44), 14499–14506.
Eroglu, S., Scholz, F., Frank, M., Siebert, C., 2020. Influence of particulate versus diffusive molybdenum supply mechanisms on the molybenum isotope composition of continental margin sediments. Geochim. Cosmochim. Acta 273, 51–69.
Fernandes, S., Mazumdar, A., Bhattacharya, S., Peketi, A., Mapder, T., Roy, R., Carvalho, M.A., Roy, C., Mahalakshmi, P., Da Silva, R., Srinivasa Rao, P.L., Banik, S. K., Ghosh, W., 2018. Enhanced carbon-sulfur cycling in the sediments of Arabian Sea oxygen minimum zone center. Sci. Rep. 8, 8665.
Froelich, P.N., Klinkhammer, G.P., Bender, M.L., Luedtke, N.A., Heath, G.R., Cullen, D., Dauphin, P., Hammond, D., Hartman, B., Maynard, V., 1979. Early oxidation of organic matter in pelagic sediments of the eastern equatorial Atlantic: suboxic diagenesis. Geochim. Cosmochim. Acta 43, 1075–1090.
Grandel, S., Rickert, D., Schluter, M., Wallmann, K., 2000. Pore-water distribution and quantification of diffusive benthic fluxes of silicic acid, nitrate, and phosphate in surface sediments of the deep Arabian Sea. Deep-Sea Res. II Top. Stud. Oceanogr. 47, 2707–2734.
Grasshoff, K., Ehrhardt, M., Kremling, K., 1983. Methods of Seawater Analysis. Verlag Chemie GmbH, Weinheim.
Grasshoff, K., Kremling, K., Ehrhardt, M., 2009. Methods of Seawater Analysis. John Wiley & Sons.
Hardisty, D., Lyons, T., Riedinger, N., Isson, T., Owens, J., Aller, R., Rye, D., Planavsky, N., Reinhard, C., Gill, B., Masterson, A., Asael, D., Johnston, D., 2018. An evaluation of sedimentary molybdenum and iron as proxies for pore fluid paleoredox conditions. Am. J. Sci. 318, 527–556.
He, Z., Clarkson, M.O., Andersen, M.B., Archer, C., Sweere, T.C., Kraal, P., Guthauser, A., Huang, F., Vance, D., 2021. Temporally and spatially dynamic redox conditions on an upwelling margin: the impact on coupled sedimentary Mo and U isotope systematics, and implications for the Mo-U paleoredox proxy. Geochim. Cosmochim. Acta 309, 251–271.
Helder, W., de Vries, R., 1979. An automatic phenolhypochlorite method for the determination of ammonia in sea- and brackish waters. Neth. J. Sea Res. 13, 154–160.
Helz, G.R., 2022. The Re/Mo redox proxy reconsidered. Geochim. Cosmochim. Acta 317, 507–522.
Helz, G.R., Vorlicek, T.P., 2019. Precipitation of molybdenum from euxinic waters and the role of organic matter. Chem. Geol. 509, 178–193.
Helz, G.R., Miller, C.V., Charnock, J.M., Mosselmans, J.F.W., Patrick, R.A.D., Garner, C. D., Vaughan, D.J., 1996. Mechanism of molybdenum removal from the sea and its concentration in black shales. Geochim. Cosmochim. Acta 19, 3631–3642.
Ho, T.Y., Quigg, A., Finkel, Z.V., Milligan, A.J., Wyman, K., Falkowski, P.G., Morel, F.M., 2003. The elemental composition of some marine phytoplankton[1]. J. Phycol. 39 (6), 1145–1159.
Ho, P., Lee, J.-M., Heller, M.I., Lam, P.J., Shiller, A.M., 2018. The distribution of dissolved and particulate Mo and V along the U.S. Geotraces East Pacific Zonal Transect (GP16): the role of oxides and biogenic particles in their distributions in the oxygen deficient zone and the hydrothermal plume. Mar. Chem. 201, 242–255.
Keil, R., Neibauer, J., Biladeau, C., Elst, K., Devol, A., 2016. A multiproxy approach to understanding the "enhanced" flux of organic matter through the oxygen-deficient waters of the Arabian Sea. Biogeosciences. 13, 2077–2092.
Kessarkar, P.M., Fernandes, L.L., Parthiban, G., Kurian, S., Shenoy, D.M., Pattan, J.N., Rao, V.P., Naqvi, S.W.A., Verma, S., 2022. Geochemistry of sediments in contact with oxygen minimum zone of the eastern Arabian Sea: proxy for palaeo-studies. J. Earth Syst. Sci. 131, 91.
Klinkhammer, G., Palmer, M.R., 1991. Uranium in the oceans: where it goes and why. Geochim. Cosmochim. Acta 55, 1799–1806.
Koho, K.A., Nierop, K.G.J., Moodley, L., Middelburg, J.J., Pozzato, L., Soetaert, K., van der Plicht, J., Reichart, G.J., 2013. Microbial bioavailability regulates organic matter preservation in marine sediments. Biogeosciences 10, 1131–1141.
Koho, K.A., de Nooijer, L.J., Reichart, G.J., 2015. Combining benthic foraminiferal ecology and shell Mn/Ca to deconvolve past bottom water oxygeantion and paleoproductivity. Geochim. Cosmochim. Acta 165, 294–306.
Kraal, P., Slomp, C.P., Reed, D., Reichart, G.J., Poulton, S., 2012. Sedimentary phosphorus and iron cycling in and below the oxygen minimum zone of the northern Arabian Sea. Biogeosciences 9, 3829–3880.
Law, G., Shimmield, T., Shimmield, G., Cowie, G., Breuer, E., Harvey, S., 2009. Manganese, iron, and sulphur cycling on the Pakistan margin. Deep-sea Res. Part II-Top. Stud. Ocean. 56, 305–323.
Lengger, S.K., Hopmans, E.C., Sinninghe Damsté, J.S., Schouten, S., 2014. Impact of sedimentary degradation and deep water column production on GDGT abundance and distribution in surface sediments in the Arabian Sea: Implications for the TEX_{86} paleothermometer. Geochim. Cosmochim. Acta 142, 386–399.
Lenstra, W., Seguret, M., Behrends, T., Groeneveld, R., Hermans, M., Witbaard, R., Slomp, C.P., 2020. Controls on the shuttling of manganese over the northwestern Black Sea shelf and its fate in the euxinic deep basin. Geochim. Cosmochim. Acta 273, 177–204.
Lenz, C., Jilbert, T., Conley, D.J., Slomp, C.P., 2015. Hypoxia-driven variations in iron and manganese shuttling in the Baltic Sea over the past 8 kyr. Geochem. Geophys. Geosyst. 16, 3754–3766.
Lewis, B.L., Luther, G.W., 2000. Processes controlling the distribution and cycling of manganese in the oxygen minimum zone of the Arabian Sea. Deep Sea Res. Part II. 47, 1541–1561.
Li, Y.H., Schoonmaker, J.E., 2003. Chemical composition and mineralogy of marine sediments. In: Mackenzie, F.T. (Ed.), Sediments, Diagenesis, and Sedimentary Rocks – Treatise on Geochemistry, vol. 7. Elsevier, Amsterdam, pp. 1–35.
Lyons, T., Severmann, S., 2006. A critical look at iron paleoredox proxies: new insights from modern euxinic marine basins. Geochim. Cosmochim. Acta 70, 5698–5722.
McManus, J., Berelson, W., Klinkhammer, G., Hammond, D., Holm, C., 2005. Authigenic uranium: relationship to oxygen penetration depth and organic carbon rain. Geochim. Cosmochim. Acta 69, 95–108.
McManus, J., Berelson, W., Severmann, S., Poulson, R., Hammond, D., Klinkhammer, G., Holm, C., 2006. Molybdenum and uranium geochemistry in continental margin sediments: Paleoproxy potential. Geochim. Cosmochim. Acta 70, 4643–4662.
Moffitt, S.E., Moffitt, R., Sauthoff, W., Davis, C., Hewett, K., Hill, T., 2015. Paleoceanographic insights on recent oxygen minimum zone expansion: lessons for modern oceanography. PLoS One 10, e0115246.
Morford, J.L., Emerson, S.R., 1999. The geochemistry of redox sensitive trace metals in sediments. Geochim. Cosmochim. Acta 63, 1735–1750.
Morford, J.L., Emerson, S.R., Breckel, E.J., Kim, S.H., 2005. Diagenesis of oxyanions (V, U, Re, and Mo) in pore waters and sediments from a continental margin. Geochim. Cosmochim. Acta 69, 5021–5032.
Morford, J., Martin, W., François, R., Carney, C., 2009. A model for uranium, rhenium, and molybdenum diagenesis in marine sediments based on results from coastal locations Geochim. Cosmochim. Acta 73, 2938–2960.
Morford, J., Martin, W., Carney, C., 2012. Rhenium geochemical cycling: Insights from continental margins. Chem. Geol. 324–325, 73–86.
Nair, T.M.B., Ramaswamy, V., Shankar, R., Ittekkot, V., 1999. Seasonal and spatial variations in settling manganese fluxes in the northern Arabian Sea. Deep-Sea Res. I 46, 1827–1839.
Nameroff, T.J., Balistrieri, L.S., Murray, J.W., 2002. Suboxic trace metal geochemistry in the Eastern Tropical North Pacific. Geochim. Cosmochim. Acta 66, 1139–1158.
Naqvi, S.W.A., Bange, H.W., Farías, L., Monteiro, P.M.S., Scranton, M.I., Zhang, J., 2010. Marine hypoxia/anoxia as a source of CH_4 and N_2O. Biogeosciences 7, 2159–2190.
Nierop, K.G.J., Reichart, G.J., Veld, H., Sinninghe Damsté, J.S., 2017. The influence of oxygen exposure time on the composition of macromolecular organic matter as revealed by surface sediments on the Murray Ridge (Arabian Sea). Geochim. Cosmochim. Acta 206, 40–56.
Olson, D.B., Hitchcock, G.L., Fine, R.A., Warren, B.A., 1993. Maintenance of the low-oxygen layer in the central Arabian Sea. Deep-Sea Res. 40, 673–685.
Passier, H., Luther, G.W., de Lange, G.J., 1997. Early diagenesis and Sulphur speciation in sediments of the Oman margin, northwestern Arabian Sea. Deep-Sea Res. II 44, 1361–1380.
Paulmier, A., Ruiz-Pino, D., 2009. Oxygen minimum zones (OMZs) in the modern ocean. Prog. Oceanogr. 80, 113–128.
Poulton, S., Canfield, D., 2005. Development of a sequential extraction procedure for iron: Implications for iron partitioning in continentally derived particulates. Chem. Geol. 214, 209–221.
Qasim, S.Z., 1982. Oceanography of the northern Arabian Sea. Deep sea research Part A. Oceanogr. Res. Pap. 29, 1041–1068.
Raiswell, R., Hardisty, D., Lyons, T., Canfield, D., Owens, J., Planavsky, N., Poulton, S., Reinhard, C., 2018. The iron paleoredox proxies: a guide to the pitfalls, problems and proper practice. Am. J. Sci. 318, 491–526.
Reichart, G.J., Lourens, L.J., Zachariasse, W.J., 1998. Temporal variability in the northern Arabian Sea oxygen minimum zone (OMZ) during the last 225,000 years. Paleoceanography 13, 607–621.
Rudnick, R.L., Gao, S., 2013. Composition of the continental crust. In: Rudnick, R.L. (Ed.), Treatise on Geochemistry, Second edition. Elsevier, pp. 1–51.
Schenau, S., Reichart, G.J., de Lange, G., 2002. Oxygen minimum zone controlled Mn redistribution in Arabian Sea sediments during the late Quaternary. Paleoceanography. 17, 3–4.
Schlitzer, R., 2015. Ocean Data View. Available online at. http://odv.awi.de.
Schmidtko, S., Stramma, L., Visbeck, M., 2017. Decline in global oceanic oxygen content during the past five decades. Nature 542, 335–339.
Scholz, F., 2018. Identifying oxygen minimum zone-type biogeochemical cycling in Earth history using inorganic geochemical proxies. Earth Sci. Rev. 184, 29–45.
Scholz, F., Hensen, C., Noffke, A., Rohde, A., Liebetrau, V., Wallmann, K., 2011. Early diagenesis of redox-sensitive trace metals in the Peru upwelling area – response to ENSO-related oxygen fluctuations in the water column. Geochim. Cosmochim. Acta 75, 7257–7276.
Scholz, F., McManus, J., Mix, A., Hensen, C., Schneider, R.R., 2014a. The impact of ocean deoxygenation on iron release from continental margin sediments. Nat. Geosci. 7, 433–437.

Scholz, F., Severmann, S., McManus, J., Hensen, C., 2014b. Beyond the Black Sea paradigm: the sedimentary fingerprint of an open-marine iron shuttle. Geochim. Cosmochim. Acta 127, 368–380.
Scholz, F., Siebert, C., Dale, A.W., Frank, M., 2017. Intense molybdenum accumulation in sediments underneath a nitrogenous water column and implications for the reconstruction of paleo-redox conditions based on molybdenum isotopes. Geochim. Cosmochim. Acta 213, 400–417.
Schulte, S., Rostek, F., Bard, E., Rullkötter, J., Marchal, O., 1999. Variations of oxygen-minimum and primary productivity recorded in sediments of the Arabian Sea. Earth Planet. Sci. Lett. 173, 205–221.
Schulz, H., von Rad, U., Erlenkeuser, H., 1998. Correlation between Arabian Sea and Greenland climate oscillations of the past 110,000 years. Nature 393, 54–57.
Scott, C., Lyons, T.W., 2012. Contrasting molybdenum cycling and isotopic properties in euxinic versus non-euxinic sediments and sedimentary Rocks: refining the paleoproxies. Chem. Geol. 324-325, 19–27.
Shimmield, G.B., Price, N.B., 1986. The behavior of molybdenum and manganese during early sediment diagenesis—Offshore Baja California. Mar. Chem. 19, 261–280.
Sinninghe Damsté, J.S., Rijpstra, W.I.C., Reichart, G.-J., 2002. The influence of oxic degradation on the sedimentary biomarker record II. Evidence from Arabian Sea sediments. Geochim. Cosmochim. Acta 66, 2737–2754.
Soetaert, K., Petzoldt, T., Meysman, F., 2010. Marelac: Tools for Aquatic Sciences. R Package Version.
Stramma, L., Johnson, G.C., Sprintall, J., Mohrholz, V., 2008. Expanding oxygen-minimum zones in the tropical oceans. Science 320, 655–658.
Sulu-Gambari, F., Roepert, A., Jilbert, T., Hagens, M., Meysman, F.J.R., Slomp, C.P., 2017. Molybdenum dynamics in sediments of a seasonally hypoxic coastal marine basin. Chem. Geol. 466, 627–640.
Tarran, G.A., Burkill, P.H., Edwards, E.S., Woodward, E.M.S., 1999. Phytoplankton community structure in the Arabian Sea during and after the SW monsoon, 1994. Deep-Sea Res. II Top. Stud. Oceanogr. 46 (3–4), 655–676.
Tribovillard, N., Lyons, T., Riboulleau, A., 2006. Trace metals as paleoredox and paleoproductivity proxies: an update. Chem. Geol. 232, 12–32.
van der Weijden, C., 2002. Pitfalls of normalization of marine geochemical data using a common divisor. Mar. Geol. 184, 167–187.
van der Weijden, C., Reichart, G.J., van Os, B., 2006. Sedimentary trace element records over the last 200 kyr from within and below the northern Arabian Sea oxygen minimum zone. Mar. Geol. 231, 69–88.
van Helmond, N.A.G.M., Jilbert, T., Slomp, C.P., 2018. Hypoxia in the Holocene Baltic Sea: comparing modern versus past intervals using sedimentary trace metals. Chem. Geol. 493, 478–490.
van Santvoort, P.J.M., de Lange, G., Thomson, J., Colley, S., Meysman, F., Slomp, C.P., 2002. Oxidation and origin of organic matter in surficial Eastern Mediterranean hemipelagic sediments. Aquat. Geochem. 8, 153–175.
Vidya, P.J., Kurian, S., 2018. Impact of 2015–2016 ENSO on the winter bloom and associated phytoplankton community shift in the northeastern Arabian Sea. J. Mar. Syst. 186, 96–104.
Wehrli, B., Stumm, W., 1989. Vanadyl in natural waters: adsorption and hydrolysis promote oxygenation. Geochim. Cosmochim. Acta 53, 69–77.
Zheng, Y., Anderson, R., van Geen, A., Kuwabara, J., 2000. Authigenic molybdenum formation in marine sediments: a link to pore water sulfide in the Santa Barbara Basin. Geochim. Cosmochim. Acta 64, 4165–4178.
Zheng, Y., Anderson, R., van Geen, A., Fleisher, M., 2002. Preservation of particulate non-lithogenic uranium in marine sediments. Geochim. Cosmochim. Acta 66, 3085–3092.